Teng Hu[1,2],Ze Yang[1,2], Zhizhong Kang[1,2,*],Hongyu Lin[3], Jie Zhong[4], Dongya Zhang[1,2], Yameng Cao[1,2], Haomin Geng[1,2]

[1] Department of Remote Sensing and Geo-Information Engineering, School of Land Science and Technology, China University of Geosciences, Xueyuan Road, Beijing, 100083 CN.

[2]Subcenter of International Cooperation and Research on Lunar and Planetary Exploration, Center of Space Exploration, Ministry of Education of The People's Republic of China, No. 29 Xueyuan Road, Haidian District, Beijing 100083 CN.

[3] Beijing Institute of Space Mechanics and Electricity, 104 Youyi Road, Beijing 100094, CN.

[4] Institute of Optics and Electronics, Chinese Academy of Sciences, Chengdu, Sichuan 610209, CN.

Corresponding author: **Zhizhong Kang** (zzkang@cugb.edu.cn)

Key Points:

- Our results show that, for the size of meter to centimeter scale impact craters, smaller craters are more degraded than larger craters.
- Images from the topographic camera confirmed that there are more small-sized craters with severe degradation in the landing area.
- The smaller the size of the impact craters, the more difficult for them to achieve impact equilibrium.

Abstract

Chang'E-4, the first soft landing mission on the far side of the Moon, provided high-resolution close-range images up to 2.3 cm/pixel, especially suitable for the study of the degradation in the population of small-sized impact craters around the landing site. This paper presents a preliminary analysis of the population degradation mechanism of the small-sized impact craters. From mosaicked descent camera image, 6316 impact craters in the landing area were extracted, identified, and classified into four types according to their morphology: complete, slightly degraded, moderately degraded, and severely degraded craters. In-situ verification using the lander topographic camera image supported the crater degradation analysis around the landing site. The small-sized impact crater population equilibrium analysis was also carried out. Over 99% of the impact craters in the study area are in degradation, which suggesting the area is severely degraded. Our results suggest that similar to the findings for impact crater populations above the meter scale, the size of meter to centimeter scale impact craters is also strongly correlated with degradation, with smaller impact craters being more likely to degrade. Images from topographic cameras also confirm the severe degradation of small-scale craters. The crater populations in equilibrium of different resolutions areas shows that the cumulative SFD slope is contrary to previous research results, the smaller the size of the impact

crater, the more difficult for them to achieve impact equilibrium, which due to secondary craters and the ground resurfacing caused by neighboring craters' ejecta.

Keywords: Chang'E-4; Landing area; Crater population degradation; Descent camera; Topographic camera; Crater impact equilibrium.

Plain Language Summary

We mosaiced the descent camera images from the Chang'E-4 mission, and identified 6316 craters in the landing area. Most of the craters are smaller than 2 meters in diameter. Then we classified all the craters to four degradation levels according to their morphology, and we also checked the corresponding craters both on the descent camera images and ground topographic camera images to verify the classified results. The statistical results show that the smaller the size of the impact craters, for diameters in the centimetre to metre scale, the more severely the crater population degradation. This is helpful for us to understand the survive time of the small-sized craters. In addition, we find that for these impact craters, the smaller the size the more difficult the impact equilibrium is to achieve, suggesting that this may be affected secondary craters and the ground resurfacing caused by the ejecta of neighboring craters.

1 Introduction

The Chang'E-4 mission was the world's first soft landing on the far side of the Moon, and is also China's second lunar surface soft landing mission (*C Li et al.*, 2021; *Liu et al.*, 2020; *Yang et al.*, 2020). The lander is equipped with a variety of cameras, capturing in-situ field images at different resolutions and different positions, providing a direct image set studies of impact craters which are smaller than 2 meters.

The impact crater is the most typical geologic feature of the lunar surface, which reveals significant information primarily regarding relative and absolute surface chronologies, erosion processes and climate history(*Geiss and Rossi*, 2013; *Hiesinger et al.*, 2012; *Massironi et al.*, 2009). Craters after formation are affected by internal and external space environments, such as micrometeorite bombardment, emplacement of ejecta from distal larger craters and internal geological deformations(*Basilevskii*, 1976; *Craddock and Howard*, 2000; *Fassett and Thomson*, 2014; *Molaro and Byrne*, 2012). The first lunar image captured from Ranger 7 confirmed the degradation of the lunar surface. As a result, their spatial morphology changes and gradually degenerates(*Wilhelms et al.*, 1987). Among the factors influencing the degradation of impact craters, direct micrometeorite bombardment and other impact crater ejecta result in incomplete craters: the lip and the rim of the impact crater disappear, and the bottom of the impact crater is filled in. Also internal geological processes such as slope processes (avalanches, taluses, landslides, creep) influence the morphology of impact craters, especially small size craters (*Basilevskii*, 1976; *Fassett and Thomson*, 2014). Some craters have sharp edges and bright ejecta, the kind we call fresh impact craters, while for others the edges are soft or incomplete, and

their walls are even collapsed and incomplete. The bottoms of these craters are filled, and their color is consistent with the surrounding background, which we call degenerate impact craters (*Craddock and Howard*, 2000; *Fassett and Thomson*, 2014; *Qiao et al.*, 2019). A degradation analysis of lunar impact crater extends and deepens existing research on crater morphology, crater identification, lunar crater history and lunar chronology (*Fassett and Thomson*, 2014). The degradation of a population of craters reflects age of the local geological units, providing insights into the processes of lunar geological evolution.

From formation to obliteration, the impact craters experience different degrees of degradation with varying degrees of morphological transformation. The state of degradation of a crater is a measure of age, reflecting the trend of development of the lunar stratum since the crater morphology changes over time; thus, crater degradation can be investigated and analyzed morphologically through crater shape-age relationship analysis.

Craddock et al. studied the crater degradation process and described the relative age of geological units through the concept of degradation parameters(*Craddock and Howard*, 2000); Basilevsky, Wood et al. and Ivanov et al. divided the degradation grade by crater morphology(*Basilevskii*, 1976; *Ivanov and Basilevsky*, 2002; *Wood et al.*, 1977); Craddock used the Clementine data to establish the degradation model and estimated the velocity of the crater degradation(*Craddock and Howard*, 2000). The equilibrium state of crater distribution was respectively studied through computer modelling (*Hartmann and Gaskell*, 1997; *Richardson*, 2009). Li used the crater data in the typical lunar mares to study the crater shape and degradation, and crater depth was used as the critical parameter of crater degradation(*K Li*, 2013).The degradation pattern of impact craters and the impact history of the region have also been studied in much detail in recent years(*Xiao and Werner*, 2015; *Xie et al.*, 2020; *Xie et al.*, 2019; *Xie et al.*, 2017). The image based ray brightness, rim and terrace sharpness, texture, crater shape and DEM data based impact crater depth, profile line, slope are the key elements of impact crater degradation analysis in existing studies, but considering the high resolution of the descent camera (cm-level resolution at the center of the landing area), in the absence of high resolution DEM, we analyze the degradation of small size impact craters mainly by the features obtained from the images(*Fassett and Thomson*, 2014; *Howard*, 2007; *Kreslavsky et al.*, 2013; *Xiao and Werner*, 2015; *Xie et al.*, 2020; *Xie et al.*, 2019; *Xie et al.*, 2017).

For the better understanding of crater degradation, an image based statistical method based on the degradation classification of impact craters was developed. Arthur defined four levels of lunar impact craters degradation(*Chapman*, 1963). Based on this we classify the degradation of the crater population into four classes based on the features available on the images, i.e. the presence of spatter patterns around the craters, the clarity of the crater edges and the contrast between the highlight and shadow of the crater interiors. Impact craters that are clear and complete, with sharp contrasting highlight and shadow in-

teriors, are considered fresh impact craters. The following impact crater types are classified according to the degree of degradation: fresh crater (C1), preliminary degraded crater (with smooth edges) (C2), crater with severely eroded forms (C3), and completely flattened Impact crater (C4). Overall, empirical measures of crater degradation levels which based on the orbiter image data are highly dependent on the appearance of impact craters, and degradation studies of small-sized craters are not supported when the resolution of orbital images is limited. Therefore, the craters in the existing studies are relatively large in size. At the same time, in the existing impact crater degradation studies, it is generally concluded that the smaller the size of the crater, the more likely it is to be filled or destroyed by subsequent impacts, while large size craters are relatively stable and less prone to degradation(*Craddock and Howard*, 2000; *Fassett and Thomson*, 2014; *Hirabayashi et al.*, 2017; *Minton et al.*, 2019; *Povilaitis et al.*, 2018) but few studies have focused on the population degradation of small size craters, especially those below the meter size. Therefore, in this study we will focus on the population degradation statistical analysis of impact craters of centimeter to meter size, which have not been addressed in previous studies. In addition, we do not analyze the effect of secondary impact craters on the degradation of impact craters because the size of the craters involved in this study is small and the distribution is dense, thus it is not possible to distinguish the primary and secondary craters by their spatial distribution patterns.

In this paper, we innovatively focus our study on the statistical analysis of the degradation of Chang'e-4 impact craters at the meter to centimeter scale. The mosaic of images from the descent camera enables our study to be completed due to the special characteristics of the descent camera images that capture an area of decreasing size and increasing resolution as the lander descends. At the same time, as Chang'e-4 is the first data to land on the lunar farside, our study is the first to obtain degradation statistics for sub-meter impact craters in the Chang'e-4 landing area. The panoramic image from the Chang'E 4 lander's topography camera was able to verify the impact craters with different degradation levels from a side-view perspective. In addition, the specificity of the descent camera images with its high central resolution and low edge resolution allows us for the first time to perform equilibrium analysis of impact crater populations at the centimeter to meter scale.

The rest of this paper is organized as follows. Section 2 introduces the study area and the data we used. Section 3 describes the used method in detail. Section 4 presents the experimental results and analysis. This paper concludes with a discussion of future research considerations in Section 5.

2 Study area and data

Chang'E-4 landed on the floor of Von Kármán crater (186 km in diameter), located in the central part of the northwestern of the South Polar Aitken (SPA) basin. Recent geological mapping surveys show that this crater is about 3.97 Ga (pre-Nectarian)(*Ling et al.*, 2019). The landing site (177.588°E, 45.457°S) (*Di et al.*, 2019)was approximately 350km northwest of the SPA ellipse center

(53°S, 169°W)(*Garrick-Bethell and Zuber*, 2009). During the landing process, the images captured by the descent camera of Chang'E-4, provided an unprecedented opportunity to study the degradation of the population of small-sized impact craters with diameter of 10m or less in the area.

We selected 25 images captured at different landing altitudes (600m to 30m). The ground resolution of the captured image increased gradually from 46 cm to 2.3 cm as the camera descended. As result of its high spatial resolution, descent camera images are ideal for interpreting the geological structures in landing areas and analyzing the geological evolution of planet surfaces. An accurate geographic reference is the foundation for mapping and interpretation of planetary geology using descent camera images. Descent cameras however, do not have geographic coordinates. Therefore, we must introduce images with geographic references to register descent camera images.

The Chang'E-2 Digital Orthophoto Map (DOM, 7 m/pixel) is the lunar global DOM with highest ground resolution, and thus used as the reference image when registering the descent camera images. The huge difference in spatial resolution between the Chang'E-2 DOM and the descent camera images however presented a serious challenge when selecting corresponding pixels. Thus, we used Lunar Reconnaissance Orbiter (LRO) high-resolution NAC image (M1298916428LR) as the intermediate transition (*Wu et al.*, 2020) .

We used full-color mosaic images, captured by the lander and published by China's Lunar and Deep Space Exploration (CLEP), containing a high-resolution topographic image of the landing zone displayed by azimuth and cylindrical projections, for the comparison of craters found in descent camera and topographic camera images

3 Methodology

As shown in Figure 1, we followed the given flow chart and analyzed the high-resolution descent camera images to explore the distribution and degradation of the population of small-sized impact craters in the landing area.

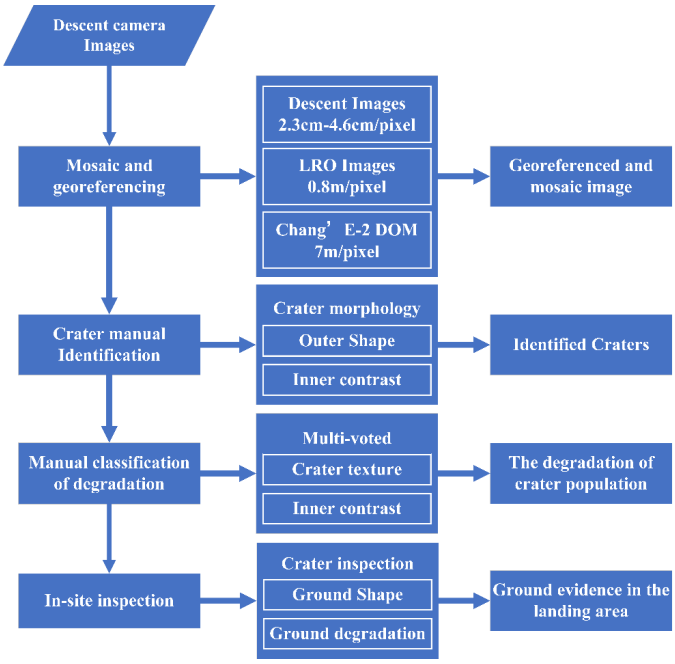

Figure.1 Flow chart of the impact craters population degradation analysis.

The descent camera images however, have no geolocation information. Thus, we needed to mosaic and register them based on existing georeferenced data. All the craters in the mosaic images were manually identified from the crater textures as the accuracy and completeness of the automatic identification techniques are limited. Craters were manually classified to different degradation levels to permit a quantitative analysis of degradation in the crater population, a multi-vote process compensated for human subjective factors. In addition, we use the lander's topographic camera to assist in verifying the correctness of the classification results. Since the main optical axis of the topographic camera is almost parallel to the lunar surface, the internal structure of the impact crater can be clearly seen from the lateral direction. Key steps of our proposed method are given in more detail in the following sub sections.

3.1 The mosaic and registration of the images from descent camera

Usually we use the SfM algorithm(*Salaün et al.*, 2017) to estimate the photo position and attitude to obtain the normalized image, but the final stage of the descent camera of Chang'e-4 lander is vertical landing, and the image is acquired along the main optical axis direction, leading to the position and attitude calculated by the SfM algorithm has a large error(*Kang et al.*, 2007; *R Li et al.*, 2002). Therefore, this paper adopts the mosaic method to obtain the mosaic images of the landing area.

Since the descent camera images lacks geo-reference, we need to register the

experimentally selected descent camera before mosaic. However, the resolution of Chang'E-2 DOM is 7m/pixel, which has a large difference with the first descent camera image (resolution 46 cm/pixel) and may lead to a large error in the registered results. Therefore, we consider using LROC NAC data to register with Chang'E-2 DOM data first and registering the descent camera images on the basis of the geo-referenced LROC NAC data. We chose about 300 pairs of corresponding pixels between Chang'E-2 DOM and the LRO image using software ArcGIS. We also randomly selected 100 pairs of pixels to count their registration errors and ensured that these pixels were evenly distributed over the experimental area. The maximum error of these 100 pairs was less than 2 pixels.

The mosaic creation process of descent images comprised three steps: image histogram equalization was carried out to improve the visual effect of the descent camera images. The corresponding pixels were selected with even distribution. One corresponding pixel was selected for every 10000 pixels (100×100 pixels), and about 100 corresponding pixels were selected between each pair of adjacent images. The cubic spline difference method was used to fit the registration model between the adjacent images. In this way, the rest 24 descent camera images were mosaicked and georeferenced. The error in registration coordinates of the randomly selected test pixel pairs (around 100 pairs of pixels) was less than 2 pixels to the LROC NAC image. The experiments selected larger size impact craters (about 50) and compared their diameters to the LROC NAC image for the difference in crater diameter. The experimental results showed that most of the craters had almost no diameter difference, with the maximum diameter difference being no more than 2 pixels. This suggests that image distortion due to data registration has little effect on subsequent crater size acquisition.

3.2 Identification of impact crater

As the most typical geomorphic structure on the lunar surface, the impact crater reveals the process of geological evolution of the moon to some extent. In this paper, the impact craters were extracted around the landing site of Chang'E-4 using manual visual identification as shown in Figures 2a and 2b. Figure 1a illustrates the contrast between the dark area (blue outline area) and the highlight area (red outline area) along the direction of illumination. Figure 2b shows the circular shape of craters (inside the red square).

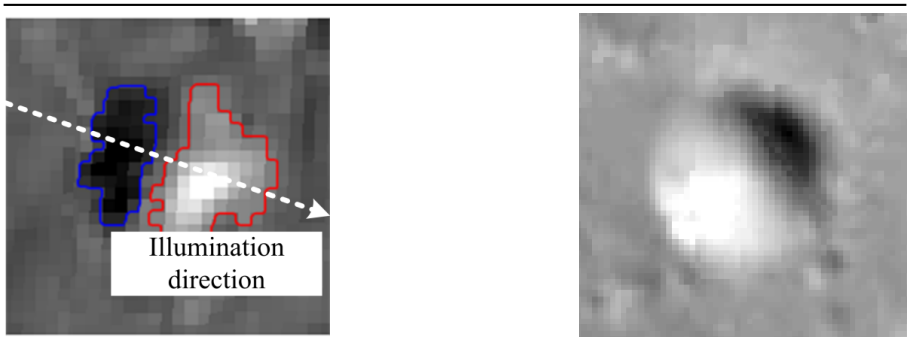

a Crescent-like highlight and shadowed regions b Circular shape

Figure.2 Visual identification criteria of impact craters features.

As shown in Figure 2, the impact crater exhibits concave relief and can be recognized in an image as a pair of crescent-like highlight and shadow areas when illuminated by sunlight from an angular direction as shown in Figure 2a. In addition, impact craters always have a local circular planform as shown in Figure 2b, so they can be distinguished from the background. Thus, craters can be identified through the combination of contrast and shape attributes. Identifying craters manually, means craters can be detected, marked, and verified through human judgment, decreasing the likelihood of incomplete and mistaken identification evident in currently deployed automatic methods.

For the identification of impact craters, a minimum crater diameter of 5 pixels or more is required, but for the degradation analysis of impact craters a minimum crater diameter of 10 or more is required due to the detailed information on the shape of the crater, the contrast between light and dark and the radiation lines around the crater.

3.3 Classification of Degradation Levels of Impact Crater

Once formed, impact craters begin to degrade gradually. The degradation process of impact craters is closely related to the internal and external lunar environment such as micrometeorite bombardment, emplacement of ejecta from distal larger craters and internal geological deformations, and the degradation of impact craters changes the morphology of impact craters(*Basilevskii*, 1976; *Craddock and Howard*, 2000; *Fassett and Thomson*, 2014; *Molaro and Byrne*, 2012). Micrometeorite bombardment can cause impact craters to be covered or filled in, while internal geological processes such as the slope process can also change the morphology of impact craters. As the degradation of the impact crater becomes more severe, the possible distal ejecta rays around the fresh impact crater gradually disappears, and the contrast between the highlights and shadows of the impact crater is no longer sharp, while the boundary gradually becomes indistinguishable and almost blends in with the surrounding lunar surface(*Fassett and Thomson*, 2014; *Huang et al.*, 2017; *Kinczyk et al.*, 2016; *Liu*

et al., 2020; *Minton et al.*, 2019). Statistical studies of morphological and other related characteristics of their degradation level are important to understand the correlation between the evolution of crater morphology and the age of the corresponding geological units. Unlike existing studies that have targeted larger size impact craters (meters and even hundreds of meters), the most of the identified craters in our study are smaller than 2 meters in diameter, unfortunately there is no DEM (digital elevation models) with a resolution higher than 0.5 meter/pixel to calculate the exact value of craters' quantitative classification indicators. Thus, a qualitative classification was applied in this paper based on traditional method(*Chapman*, 1963). As shown in Figure 3, we used a qualitative identification method to define and determine the degradation levels of impact craters. These were divided into four types (C1-C4):

1) C1 type: fresh craters, with obvious radiation lines or the clear edge, and the highlight and shadow contrast is sharp;

2) C2 type: slightly degraded craters, the edge is clear, and the contrast between highlight and shadow is relatively clear;

3) C3 type: moderately degraded craters, shows clear signs of degradation with small highlight and shadow difference, crater floors being are raised with a filling effect, and fuzzy circular outlines;

4) C4 type: severely degraded craters; their outline is unclear, the crater floors are shallow, and the circular outline of the foundation can be distinguished when the image is stretched.

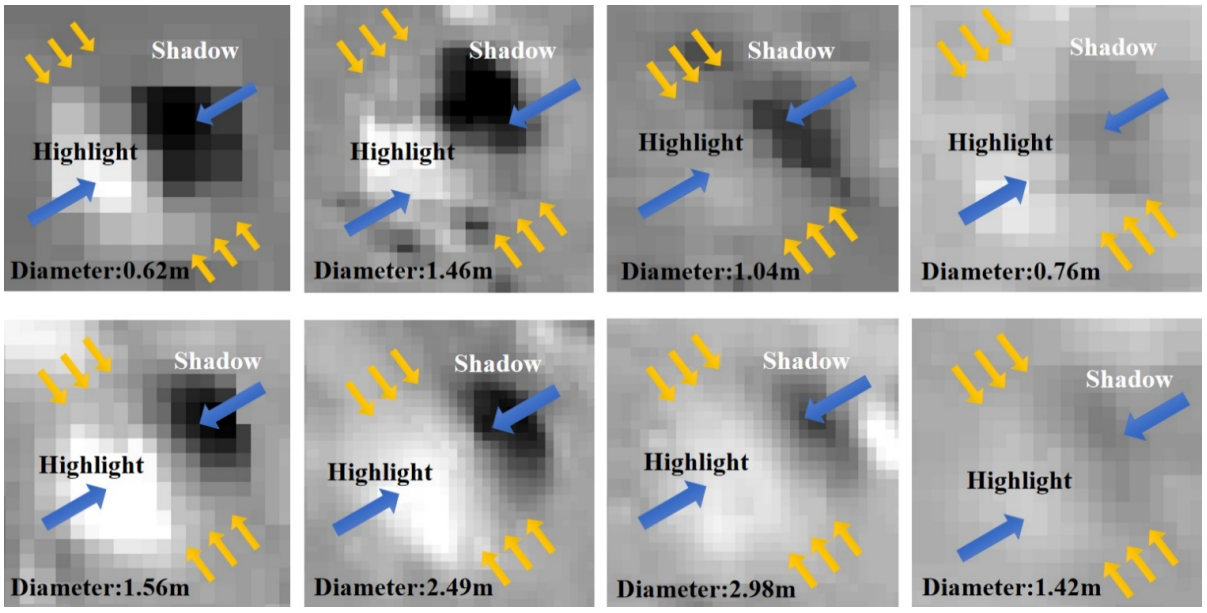

C1 C2

Figure. 3 Examples of craters at four degradation levels. Blue arrows mark the shaded and highlighted areas of the impact crater, yellow arrows mark the impact crater boundary. The diameters of the impact craters shown are also marked on the figures.

The manual qualitative classification of craters usually introduces human subjective factors, so judgment errors are inevitable. For example, the C3 type craters in Figure 3c are similar to C4 type craters and may be misclassified, so a multi-voting process for all craters was adopted. Zhang, Dong and Geng classified all the craters independently, and the votes were combined for each crater. The inconsistent results were discussed and determined collaboratively.

3.3 Comparative analysis of topographic and the descent camera images

We compared craters in images from both the topographic and the descent cameras. We identified the corresponding craters manually in both types of images and analyzed the degradation of the crater population in the landing area. We verified our results by comparing the identified craters on the descent camera images to the corresponding craters on the topographic camera images. Figure 4 shows two pair of corresponding craters (blue circle and red circle) on descent camera images and topographic camera images.

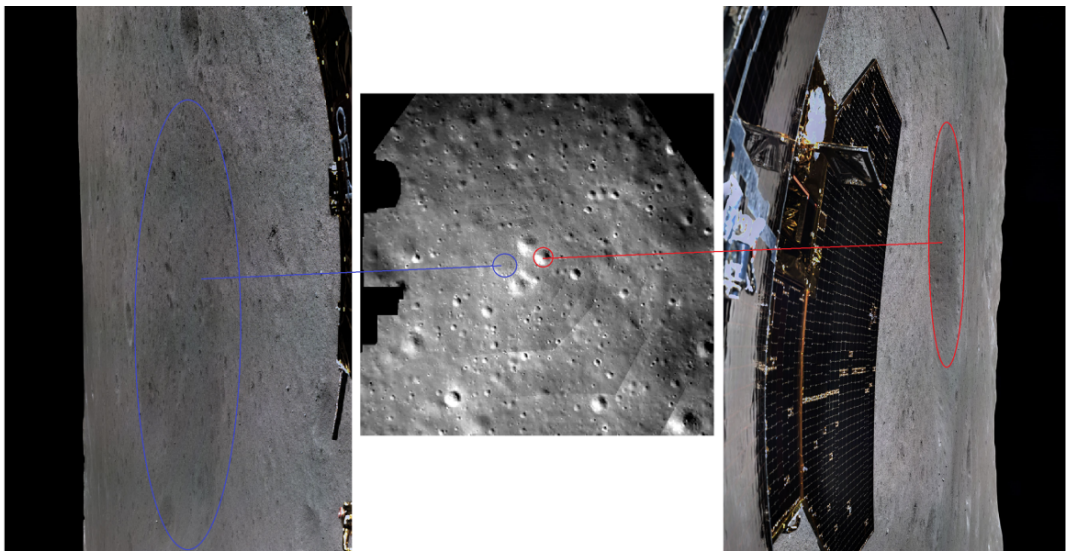

a b c

Figure. 4 The comparison of impact craters on the descent camera image (b) and the topographic camera images (a and c; cylindrical projection). Red line circled areas are a pair of corresponding easily identified impact craters and the blue line circled areas are a pair of corresponding severely degraded and

hard-identified impact craters.

As shown in Figure 4, one easily identified and one severely degraded crater appear on the descent and topographic camera images. After we manually identified these two craters on the mosaic of descent camera images, we analyzed the image of the craters in mosaic to the topographic images for close-sight verification. We compared the craters from different angles. In the central part of landing area, the exact degradation levels and actual spatial forms of some craters were checked one by one at close range. This comparison helped us to understand the actual morphology of craters in the descent camera images.

4 Results

4.1The mosaic of the descent camera images

Based on the images of the Chang'E-4 descent camera, we selected 25 images captured in different heights for the mosaic of the landing area. The result is shown in Figure 5.

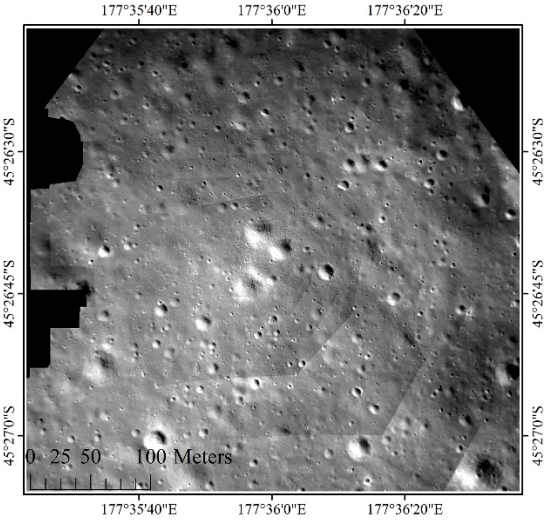

Figure. 5 The mosaic of Chang'E-4 descent camera images.

The study area centering on the landing point was defined, covering an area of 151,797 m2 (407 m from east to west and 385 m from north to south) as shown in Figure 5. The descent images used in this paper were captured along the optical axis during the landing process, so the size of the extractable impact craters gradually decreases as the ground resolution of the descent camera images rises, especially in the central landing area where the extractable size can reach the decimeter level. Due to the enhanced spatial resolution, miniature impact craters with diameter of 15 cm could be identified over the central landing area. Thus, the descent camera images provided a reliable data source for analyzing impact craters around the landing site. As seen in the image, there were numerous impact craters around the landing site.

4.2 Impact Crater Distribution Results

In total, 6316 impact craters were identified and extracted manually. The crater distribution map is shown in Figure 6, the crater density map is shown in Figure 7 and the boundaries of different sized craters are circled in Figure 8.

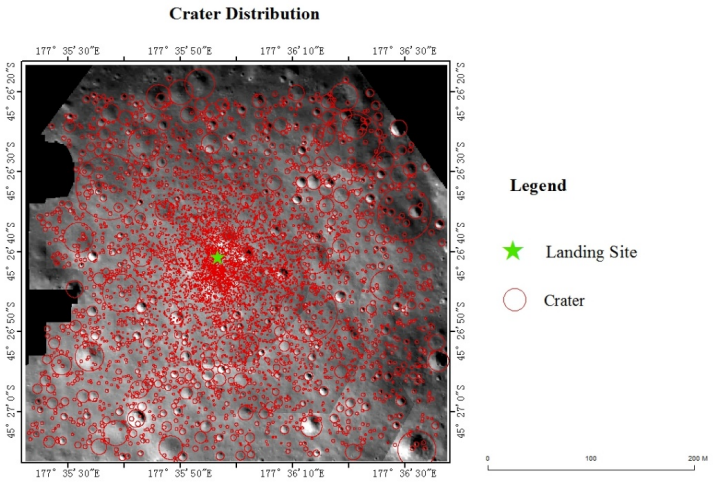

Figure.6 The impact craters distribution map.

As shown in Figure 6, there were many craters in the landing zone covering a large surface area with a relatively concentrated distribution. Around the landing site (the green pentagram), most are concentrated small-sized craters. The craters located in the marginal area are relatively larger than the craters found in the central area as the image ground resolution decreased with distance from the central area.

Since the region closer to the center of the mosaic descent image has higher resolution, the distribution of impact craters is also denser. Therefore, we divide the degraded impact craters into several zones in the subsequent analysis and partition the degradation of impact craters in these zones into statistics. The Red/yellow/aquamarine outline areas contains craters smaller than 0.5m/1m/2m in diameter.

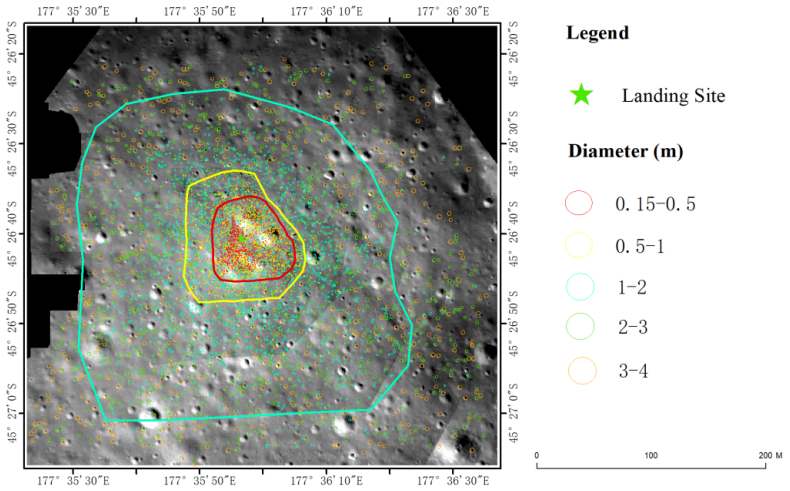

Figure.7 The boundaries of different sized impact craters observed by the descent camera. The Red/yellow/aquamarine outline areas contains impact craters smaller than 0.5m/1m/2m in diameter, as constrained by the limitations of the resolution of images from descent camera.

As shown in Figure 7, the boundaries of detectable small-sized craters are indicated by outlines in the landing area. As many as 2,600 craters with a diameter less than 1 m were extracted within 50 m from the landing point, showing a very high crater density. Among them, 975 craters with a diameter of 0.15m-0.5m were only reflected in the range of 30m around the landing site, while the distribution of craters with a diameter of 0.5m-1m was further expanded, showing the close contact between the crater extraction size and the image spatial resolution. The outer region did not extract a smaller size impact crater because the image resolution limited the further extraction and recognition of the miniature impact crater.

As a special property of the descent camera mosaic image, the mosaic image is high resolution at the center and lower resolution towards the image boundary. The red line area therefore has the highest resolution (0.023m/pixel), and the resolution of the edge portion of the mosaic data is 0.632m/pixel. The identification of impact craters requires 5 pixels, but considering the degradation features of impact craters, a minimum of 5 pixels (10 pixels for most) is required to identify them. As a result of this we obtained a population of small impact craters with a diameter of 0.15m-67m. The minimum impact crater diameter required to allow impact crater degradation analysis in the red line area is 0.15m. The size and frequency of the impact craters red/yellow/aquamarine/entire areas of Figure 7 are shown in Table 1.

Table.1 Size and frequency of impact craters in the landing area.

Region\ count	-0.5m (#)	-1m (#)	-2m (#)	-4m (#)	-6m (#)	-12m (#)	-20m (#)	-70m (#)
Red outline (4956 m^2)								
yellow outline (10943m^2)								
Aquamarine outline (82069.05m^2)								
Entire (151797 m^2)								

Table 1 shows the size and frequency of the craters in different crater-size-limited region in the landing area. The craters in each area tended to gradually increase as the size becomes smaller. Impact craters showed an inverse proportional relationship between size and frequency. The smaller the crater size, the higher the frequency, while the larger the crater size, the lower the frequency.

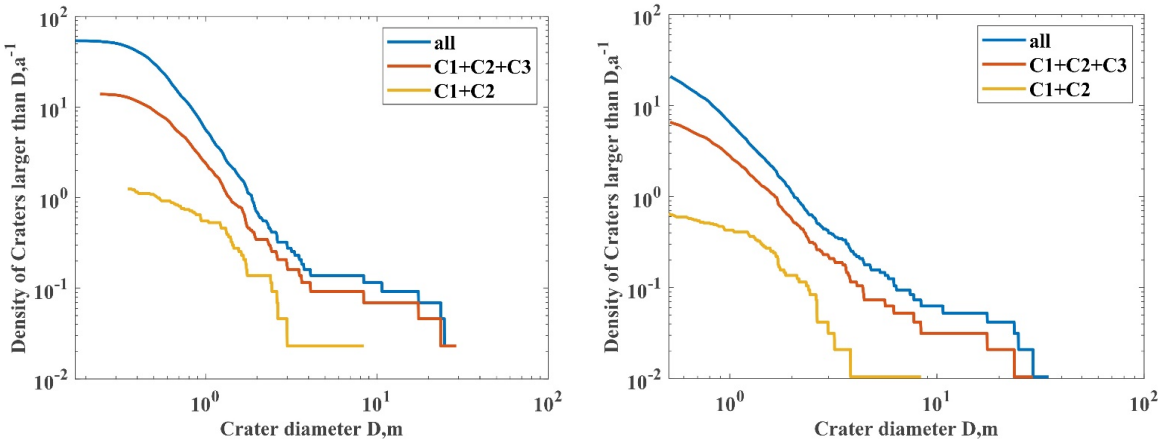

(a) (b)

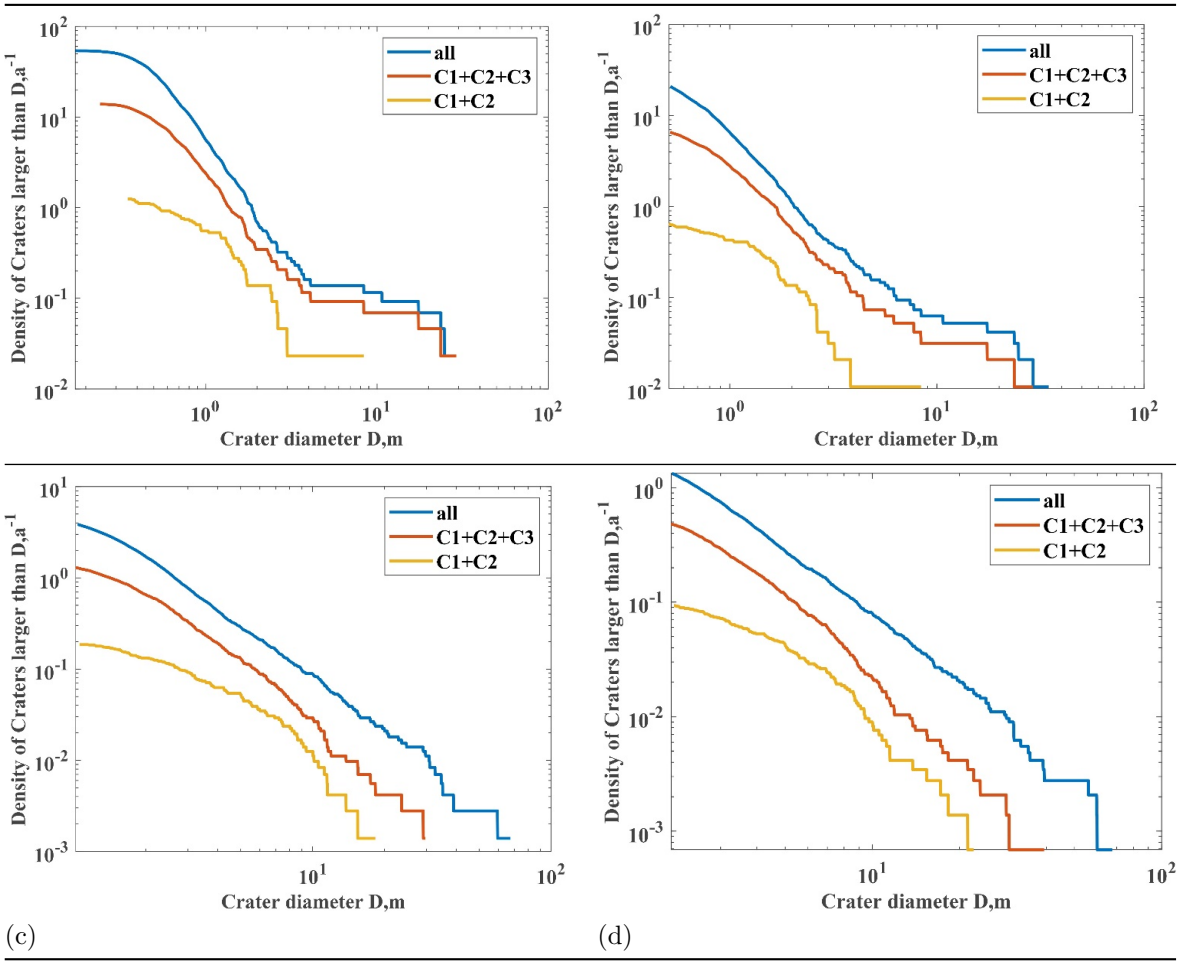

Figure.8 Cumulative distribution of combined craters in different statistical areas. Fig. 8 a/b/c/d are C1+C2/C1+C2+C3/all craters' distribution in the Red/yellow/aquamarine outline and entire areas.

As shown in Fig.8, four crater cumulative distribution curves shows the similar distribution shape. The number of impact craters gradually decreases as the size increases in all statistical areas, but kinks appear in all the distribution curves. The kinks for C1+C2/C1+C2+C3/all craters' distribution in Figure 8a/b/c/d is 3/4/4 meter, 4/8/8 meter, 10/11/12 meter and 10/10/12 meter. As the statistical area gradually becomes larger, the crater size corresponding to the kink point gradually becomes larger, and nearly disappeared in Figure 8d.

4.3 Impact crater degradation and crater size

All the craters in the landing area were classified according to the spatial mor-

phology of the impact craters. For the completeness of the identified results, wo analyzed the craters according to the distribution of craters. The statistical areas with the classified craters are visualized in Figure 9 and Figure 10, Detailed degradation results for the crater population are given in Table 2.

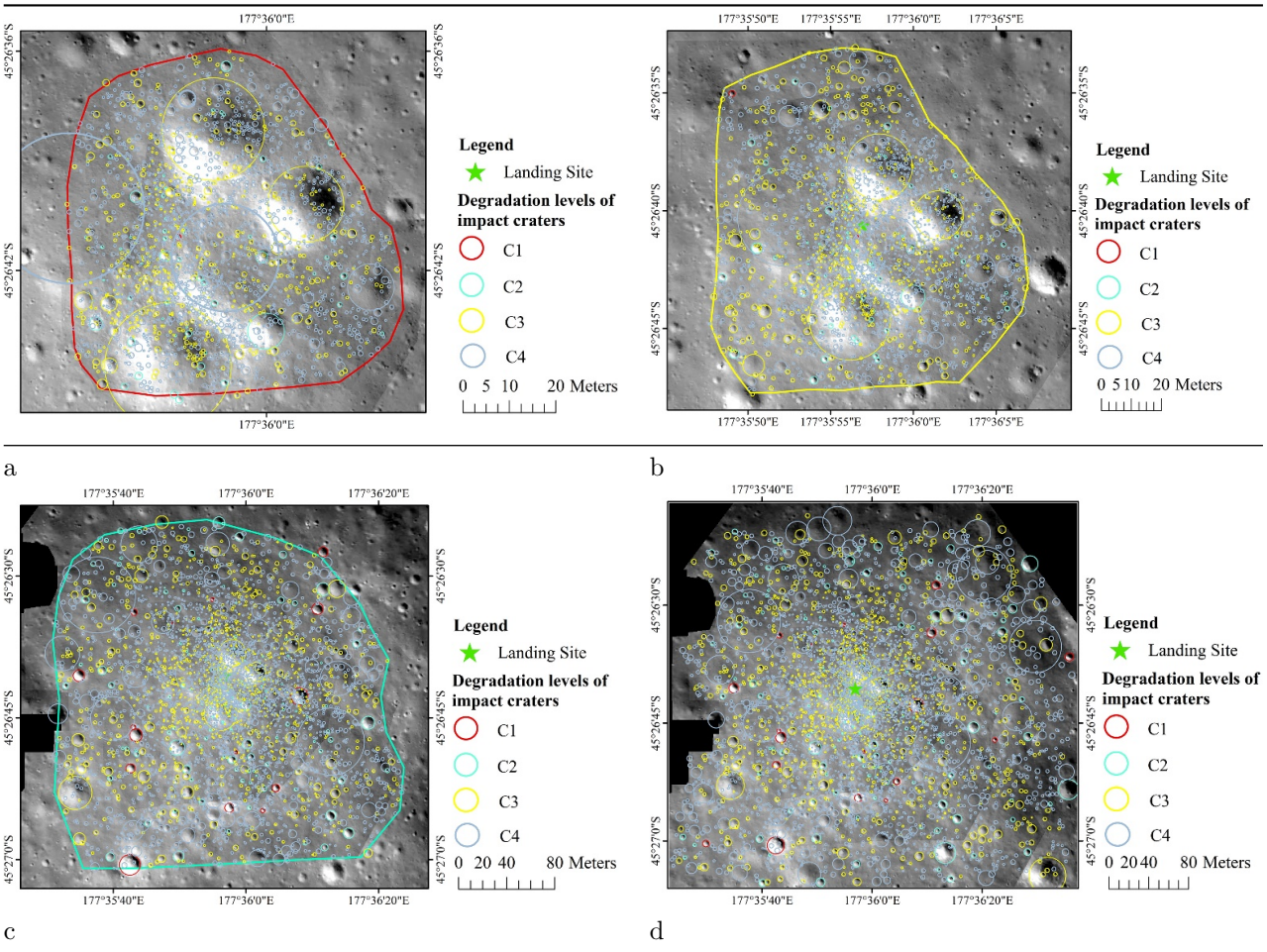

Figure.9 Crater distribution map with different degradation levels in different statistical areas. Fig.9a to Fig.9c are red/yellow/aquamarine outlined statistical area. Fig. 9d is the entire landing area. Red/aquamarine/yellow/gray circles are C1/C2/C3/C4 impact craters.

As shown in Figure 9 that the C1 craters (red, fresh craters) in all four statistical areas were rare and the distribution was sparse. C2 impact craters (aquamarine, slightly degraded craters) covers more area than C1 craters. C3 craters (yellow, moderately degraded craters) and C4 craters (gray, severely degraded craters) extended over a large range of the landing area. Thus, the impact craters in the

landing area were dominated by C3 and C4 impact craters, occupying most of the landing area.

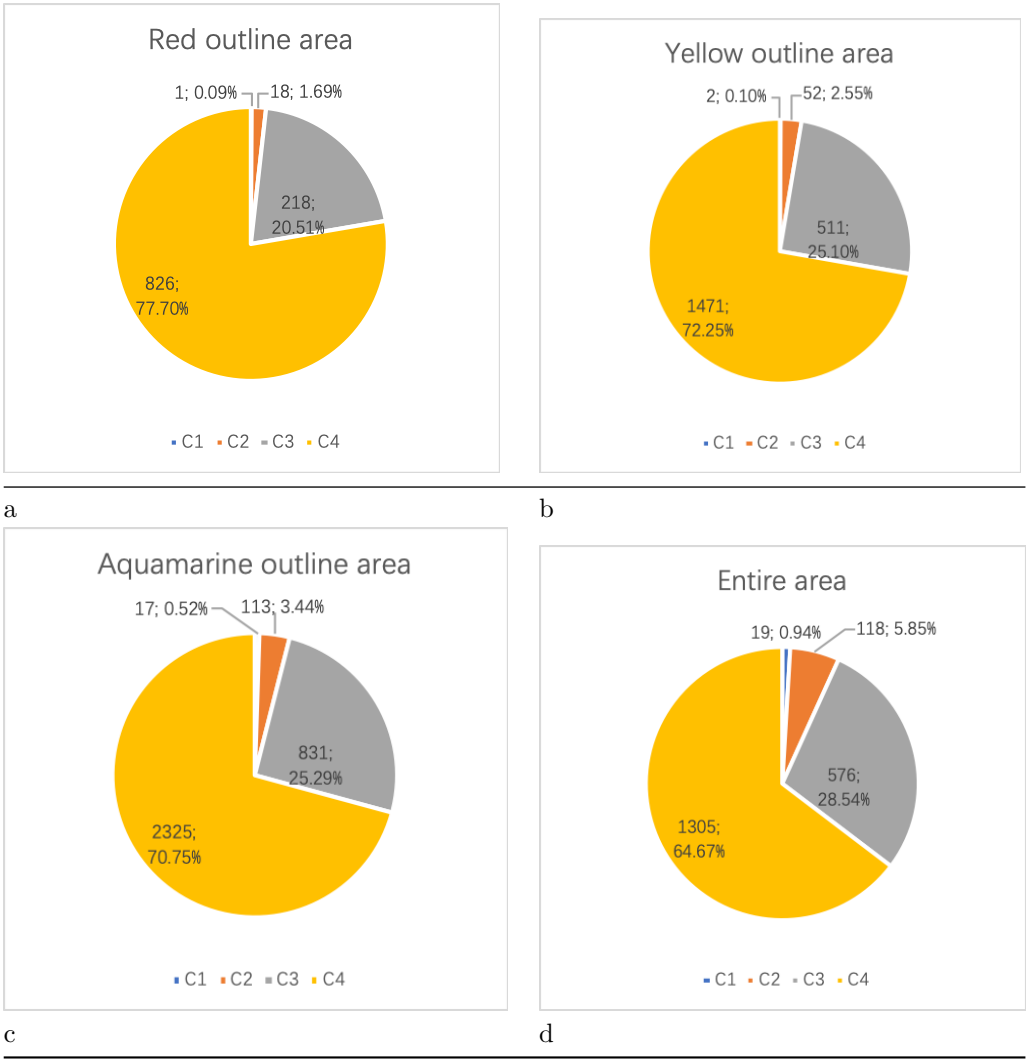

Figure.10 The degradation statistics of impact craters in different statistical areas.

As shown in Figure 10, the C1 (blue) craters are very few in all four charts, and the proportions of C2-C4 are gradually increasing, especially the proportions of C4 craters (yellow) were all extremely high (exceeded 60%). There are only 19 C1 craters in the entire landing area, so the rest 6297 craters have different degrees of degradation.

We analyzed the degradation of craters population with a number larger than 10 craters based on Table 1 to make the statistics representative. The results are shown in Table 2.

Table.2 Landing area crater population by crater size and degradation

Region\size	0.5m	-1m	-2m	-4m	-6m	-12m	-20m	-70m
Red outline (4956 m^2)	total							
	C1	%	%	%				
		0.82%	3.41%	6.67%				
		19.49%	31.42%	33.33%				
		79.69%	65.17%	58.67%				
	C2							
	C3							
	C4							
yellow outline (10943m^2)	total							
	C1		%	%	%			
			1.48%	6.00%	13.95%			
			23.02%	32%	39.53%			
			75.51%	61.71%	44.19%			
	C2							
	C3							
	C4							
Aquamarine outline (82069.05m^2)	total							
	C1			%	%	%	%	%	%
				2.30%	4.04%	10.22%	12.28%	4.35%	6.25%
				26.31%	29.53%	33.87%	29.82%	4.35%	6.25%
				71.33%	66.01%	53.76%	51.75%	82.60%	81.25%
	C2							
	C3							
	C4							
Entire area (151797 m^2)	total							

Region\size	-1m	-2m	-4m	-6m	-12m	-20m	-70m	
0.5m								
C1				%	%	%	%	%
				4.01%	8.36%	13.94%	4.17%	6.45%
				28.52%	32.31%	28.85%	10.42%	12.90%
				67.18%	58.56%	52.88%	81.25%	80.65%
C2								
C3								
C4								

As shown in Table 2, the red and yellow lines area provide the impact crater degradation in the intervals [0.15m,2m] and [0.5m,4m] for impact crater diameters, respectively. For both areas, C1 has the lowest percentage of impact craters, while C4 has the highest percentage of impact craters. Besides, for those areas, the smaller the impact crater diameter, the fewer the C1-C3 impact craters and the more the C4 impact craters. In addition, as the crater diameter increases, the proportion of C1-C3 impact craters increases while the proportion of C4 impact craters decreases (for the red line area decrease from 79.69% to 58.67% and for the yellow line area decrease from 75.51% to 44.19%). This suggests that the smaller the diameter of the impact crater population the more degraded they are.

Aquamarine outlined area provides the degradation of craters with the size from 1m to 70m in diameter, and the entire area show the degradation of craters from 2m to 70m in diameter. The craters smaller than 12m in diameter, show gradual increased ratios of C1 and C2 craters, and also the gradual decreased ratios of C4 craters. But the ratio of the C3 craters in size interval [6m-12m] decreased, seems that the proportion of C1 and C2 craters were increased enough to influence the C3 craters. In size interval [12m, 20m] and [20m, 70m], the C4 ratio was the highest, but their numbers were no more than 50. We believe that the range of the landing area limited the identified samples of the crater larger than 12m, thus showing a different statistical rule from the other size intervals.

In the above paper, we have innovatively analyzed the degradation pattern of populations of small impact craters (0.15cm-67m diameter) at the meter and even centimeter-scale extracted from descent camera mosaic data. It is found that the overall population of impact craters in this size range also shows a trend towards more severe degradation with smaller crater sizes. The specific degradation of these small impact crater populations is summarized as follows:

1. For each experimental area, the proportion of C4 type impact craters is the highest, exceeding 50% for most areas, and the proportion of fresh impact craters is less than 10%, indicating that the impact crater degradation in the Chang'e-4 landing area is severe. Since the size of the craters in the landing area was relatively small (the maximum diameter was 67m), it could be seen that these craters were formed by small objects hitting the

ground of the landing area. Due to the limited impact energy, there was no violent material melting process, resulting in a limited size of the crater formed. Compared to large-sized craters, the material of the small crater walls was also limited in strength and more susceptible to degradation.

2. As the size of the impact crater increased, the proportions of C1, C2 and C3 craters, are all gradually increased, while the proportion of C4 craters was gradually decreased. The similar rules can be seen in four statistical areas, especially the craters smaller than 12m in diameter. This suggests that the smaller the size of the impact crater the more severe the degradation.

4.4 In-situ inspection results

In this paper, we used the topographical camera images from Chang'E-4 lander for in-situ inspection, the results are shown in Figure 11 and Figure 12.

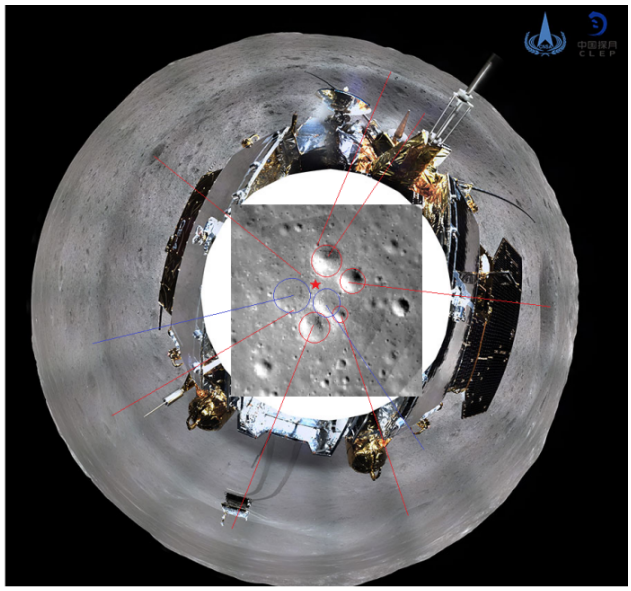

Figure.11 The comparison of images from descent camera and topographic camera. (Lander topographic images are from the CLEP network (http://www.clep.org.cn/n5982341/c6805144/content.html), the line shows the corresponding craters, the five-pointed stars are the landing point.)

As shown in Figure 11, the topographical camera image (azimuth projection) was in agreement with the descent camera's images, and the main impact craters in the ring image was well reflected. There are six relatively large craters at the landing site. The red craters were easily identified craters seen in the descent camera image, and clearly reflected in the lander topographical camera image. The blue craters were two severely degraded craters in the descent images, with topographic relief shape in topographical camera image, but the lips of these

two impact craters disappeared, with severe internal filling, leaving only the initial circular shapes. This helped us to understanding the gradated craters in a close range with a different visual angle.

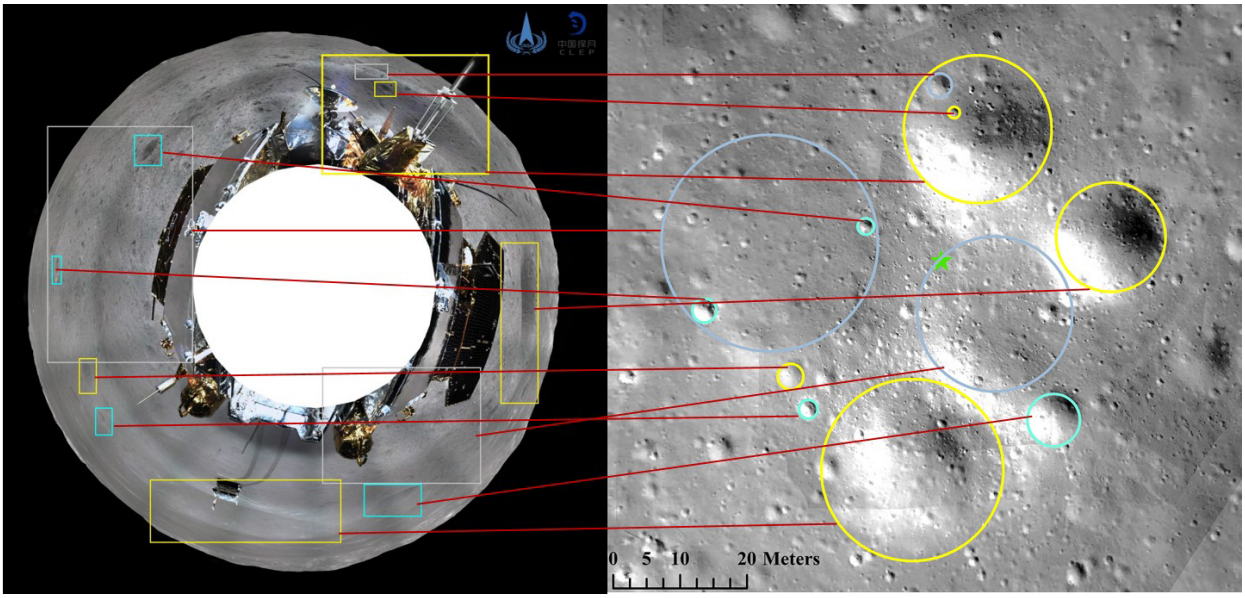

Figure.12 The corresponding classified impact craters on the topographic and descent camera images. The red lines show 12 corresponding craters with difference degradation levels. Aquamarine/yellow/gray circles are C2/C3/C4 impact craters.

As seen in the Figure 12, 12 pairs of corresponding craters (four C2, five C3 and three C4 craters) on the topographic and descent camera images are linked by red lines. C2 craters (aquamarine) have clear circular shape, and the inner contrast between highlight and shadow is clear on the topographic camera images. C3 craters (yellow) have circular shape but the crater lips have no obviously ground protrusion. C4 craters (gray) have hidden circular shape, the inner bottoms were infilled, and the crater lips are disappeared. Those classified degradation levels on the descent camera images were in consistent with the topographic camera images.

Moreover, there were a large number of impact craters with different sizes around the landing point, with varying forms of degradation. Most of the craters on the ground are small-sized craters, and their distribution was dispersed across the surface, and consistent with their distribution in the descent images. However, only few small craters had a clear circular shape. Most of the miniature impact craters were severely degraded; and their resistance to degradation was weak and gradually disappearing. That was the reason why craters with a diameter of less than 0.5 m have a higher C4 ratio in distribution analysis results, table 2.

5 Discussion

With continuous bombardment, the crater density of any diameter impact crater eventually reaches an upper limit, especially for small impact craters(*Melosh*, 1989; *Richardson*, 2009). An impact crater population is considered to be in equilibrium when the production rate of craters smaller than a given diameter in the impact crater population is balanced by the removal rate(*Xiao and Werner*, 2015). Impact crater-based lunar surface age determinations should always be performed on impact crater populations larger than the equilibrium onset diameter(*Gault*, 1970).

The images acquired by the Chang'e-4 lander's descent camera has the characteristic of higher resolution the closer it is to the ground, while the Chang'E-4 mission itself is landing on the farside of the Moon, allowing us to acquire images of different resolutions of the Chang'e-4 landing areas on the lunar farside, so we have divided the experimental data into four study areas above. Impact craters larger than 5x pixels were identified for each study area based on the different resolutions of the study areas and combined with the need for degradation analysis. We calculated cumulative SFD slopes for each experimental area based on power-law exponents (power law exponents is less than the cumulative slope by 1 and the equilibrium onset diameter for the impact craters in the different experimental areas shown in Table 3 (*Group et al.*, 1979). The experimental results show that for the smaller the experimental area and the higher the resolution, the greater the cumulative SFD slope and the smaller the onset diameter of impact equilibrium.

In previous studies, the cumulative SFD slope for impact equilibrium of 2, while the production SFD slope of 3.(*Gault*, 1970; *Xiao and Werner*, 2015).In contrast, only the cumulative SFD of the impact crater population in the entire area of our study is about 2, a parameter that has been considered to be in equilibrium in previous studies, while the equilibrium onset diameter of the impact crater in this area is 3m. For impact crater populations with higher resolution and smaller diameter ranges the red line area, the yellow line area, and the Aquamarine outline area are found to have the highest resolution areas with steeper cumulative SFD slope (red outline area 2.69, yellow outline area 2.39, aquamarine outline area 2.33). In previous studies, smaller diameter impact crater populations were more likely to reach equilibrium(*Xiao and Werner*, 2015), thus the red outline area should be the most likely of the study areas to be in equilibrium. However, the red outline area has the highest cumulative SFD slopes seems the statistical area is far from crater equilibrium, while the large areas are easy to reach equilibrium.

Table 3. Summary of the Equilibrium States of the Crater Populations on the Counting Areas

Counting Areas	Cumulative SFD slopes	D_{eq}(m)
Red outline area	2.6962	0.7789

Counting Areas	Cumulative SFD slopes	D_{eq}(m)
yellow outline area	2.3918	0.8102
Aquamarine outline area	1.9522	2.0899
Entire all	1.9165	3.0370

As for the inconsistency of our findings relative to previous impact crater population equilibrium studies, we also suggest that it is possible that the Chang'e-4 landing area has a very old stratigraphy(*Qiao et al.*, 2019) , as well as a thick lunar soil thickness, and thus may have a large distribution of secondary impact craters. Such secondary impact craters may be more widely distributed at the centimeter diameter range. A large distribution of secondary impact craters would result in a steeper cumulative SFD slope(*Xiao and Strom*, 2012) resulting higher resolution area has a steeper cumulative SFD slope.

In the other hand, taking the inflection points in the crater distribution curves in Fig. 8 into account, it seems that some magma resurfacing events happened in the landing area, resulting in part of small craters were infilled and disappeared in the crater counting results. But the recent research (*Di et al.*, 2019) shows that the landing zone is 70 meters higher than the surrounding lunar basalt, and the ground minerals were mainly ejected from Finsen and Alder craters. So, the ground is not infilled by magma.

The kink for C1+C2/C1+C2+C3/all craters' distribution shown in Figure 8 is 3/4/4 meter, and the crater excavation depths can be scaled by diameters (0.084:1 for simple craters (*Melosh*, 1989; *Thomson et al.*, 2009)), thus the depth for a crater with a diameter of 4 meters will be 33.6 cm. Considering the existence of 5 Craters with a diameter of 15-22m in the red statistical area, and their different degradation levels, these 5 impact craters were formed at different times. During the impact formation process, the materials were ejected to the surrounding area, thereby covering the neighboring tiny craters produce an effect similar to magma resurfacing events. This ejecta reshaping process may have caused the reduction in the number of crater smaller than 4m in diameter in red statistical area. Then, the cumulative curve of impact craters terminates the impact equilibrium state and turn to the process of crater accumulation. As the statistical area gradually becomes larger, the crater size corresponding to the kink point gradually becomes larger shown in Figure 8 , and nearly disappeared in Figure 8d. This shows that the surface was more and more difficult to be resurfaced by ejecta minerals as the craters get larger, and this is likely the reason that the inflection point of the statistical curve of impact craters gradually increases until it disappears.

Considering that the smaller the impact crater mentioned above, the more serious the degradation, thus, the smaller the size of the impact crater, the more difficult for them to achieve impact equilibrium, due to secondary craters and the ground reshaping caused by neighboring craters' ejecta.

6 Conclusion

In this paper, a mosaic image at high-resolution was acquired using the optical images from Chang'E-4 descent camera and 6316 craters with diameter from 0.15m to 67m were manually extracted and classified into different degradation levels. The special characteristics of Chang'e-4 descent camera image have allowed us to obtain the degradation of a centimeter to meter impact craters in the Chang'e-4 landing area on the lunar farside for the first time, whereas previous studies have mainly focused on the degradation analysis of 100-meter impact craters, and few have done impact crater populations below the meter scale. For these centimeters to meter impact craters, most of them belonged to medium-degraded and severely degraded impact craters; we infer that the smaller the crater size, the more severe the degradation in the entire crater population, which is similar to the degradation pattern of large impact craters. Images from the topographic camera on the lander confirm these results. Unlike previous findings, the smaller diameter impact crater populations have steeper SFD slopes, which may be due to secondary craters and the ground reshaping caused by neighboring craters' ejecta. In the future, we will use a wide range of high-resolution images of landing areas, combined with a variety of in-situ images collected by rover cameras, obstacle-avoidance cameras, and navigation cameras to study the degradation of the small-sized craters far away from landing site, further.

Acknowledgments

- The Chang'E-4 mission was carried out by the Chinese Lunar Exploration Program, and the data can be downloaded from the Data Release and Information Service System of China's Lunar Exploration Program (https://moon.bao.ac.cn/ce5web/searchOrder_dataSearchData.search). The mosaic of Chang'E-4 descent camera images and all 6316 classified craters can be found on http://zenodo.org/record/3600427.
- This work was supported by National Natural Science Foundation of China (Grant Nos. 41602215, 41872207), the Fundamental Research Funds for the Central Universities (2-9-2017-106), National Key R&D Program of China (Grant No. 2020YFE0202100), and the 2021 Graduate Innovation Fund Project of China University of Geosciences,Beijing(ZY2021YC008).

References

Basilevskii, A. T. (1976), On the evolution rate of small lunar craters, *Lunar Planetary Science Conference Proceedings*, *7th*, 1005-1019.Chapman, C. (1963), The system of lunar craters, *Quadrant I., Comm*, *2*(30), 71-78.Craddock, R. A., and A. D. Howard (2000), Simulated degradation of lunar impact craters and a new method for age dating farside mare deposits, *Journal of Geophysical Research: Planets*, *105*(E8), 20387-20401.Di, K., M. H. Zhu, Z. Yue, Y. Lin, W. Wan, Z. Liu, S. Gou, B. Liu, M. Peng, and Y. Wang (2019), Topographic evolution of Von Kármán crater revealed by the lunar rover Yutu-2, *Geophysical Research Letters*, *46*(22), 12764-12770.Fassett, C. I., and B. J. Thomson

(2014), Crater degradation on the lunar maria: Topographic diffusion and the rate of erosion on the Moon, *Journal of Geophysical Research: Planets*, *119*(10), 2255-2271.Garrick-Bethell, I., and M. T. Zuber (2009), Elliptical structure of the lunar South Pole-Aitken basin, *Icarus*, *204*(2), 399-408.Gault, D. E. (1970), Saturation and equilibrium conditions for impact cratering on the lunar surface: Criteria and implications, *Radio Science*, *5*(2), 273-291.Geiss, J., and A. P. Rossi (2013), On the chronology of lunar origin and evolution, *The Astronomy and Astrophysics Review*, *21*(1), 68.Group, C., R. E. Arvidson, J. Boyce, C. Chapman, and R. Young (1979), Standard techniques for presentation and analysis of crater size-frequency data, *Icarus*, *37*(2), 467-474.Hartmann, W. K., and R. W. Gaskell (1997), Planetary cratering 2: Studies of saturation equilibrium, *Meteoritics & Planetary Science*, *32*(1), 109-121.Hiesinger, H. v., C. Van Der Bogert, J. Pasckert, L. Funcke, L. Giacomini, L. Ostrach, and M. Robinson (2012), How old are young lunar craters?, *Journal of Geophysical Research: Planets*, *117*(E12).Hirabayashi, M., D. A. Minton, and C. I. Fassett (2017), An analytical model of crater count equilibrium, *Icarus*, *289*, 134-143.Howard, A. D. (2007), Simulating the development of Martian highland landscapes through the interaction of impact cratering, fluvial erosion, and variable hydrologic forcing, *Geomorphology*, *91*(3-4), 332-363.Huang, Y. H., D. A. Minton, M. Hirabayashi, J. R. Elliott, J. E. Richardson, C. I. Fassett, and N. E. Zellner (2017), Heterogeneous impact transport on the Moon, *Journal of Geophysical Research: Planets*, *122*(6), 1158-1180.Ivanov, M., and A. Basilevsky (2002), Morphology and size–frequency distribution of kilometer-scale impact craters on Callisto and Ganymede derived from Galileo data, *Solar System Research*, *36*(6), 447-457.Kang, Z. Z., Z. X. Zhang, and F. L. Yang (2007), Relative Orientation and Epipolar Arrangement based on Forward Moving Image Pairs along the Optical Axis, *Acta Geodaetica et Cartographica Sinica*, *36*(1), 56-61.Kinczyk, M., L. M. Prockter, C. R. Chapman, and H. Susorney (2016), A Morphological Evaluation of Crater Degradation on Mercury: Revisiting Crater Classification with MESSENGER Data, paper presented at 46th Annual Lunar and Planetary Science Conference.Kreslavsky, M. A., J. W. Head, G. A. Neumann, M. A. Rosenburg, O. Aharonson, D. E. Smith, and M. T. Zuber (2013), Lunar topographic roughness maps from Lunar Orbiter Laser Altimeter (LOLA) data: Scale dependence and correlation with geologic features and units, *Icarus*, *226*(1), 52-66.Li, C., W. Zuo, W. Wen, X. Zeng, X. Gao, Y. Liu, Q. Fu, Z. Zhang, Y. Su, and X. Ren (2021), Overview of the Chang'e-4 mission: Opening the frontier of scientific exploration of the lunar far side, *Space Science Reviews*, *217*(2), 1-32.Li, K. (2013), Study on Small-Scale Lunar Craters' Morphology and Degradation, Wuhan University, Wuhan, China.Li, R., M. Fei, F. Xu, L. H. Matthies, C. F. Olson, and R. E. Arvidson (2002), Localization of Mars rovers using descent and surface-based image data, *Journal of Geophysical Research Planets*, *107*(E11), FIDO-1-FIDO 4-8.Ling, Z., L. Qiao, C. Liu, H. Cao, X. Bi, X. Lu, J. Zhang, X. Fu, B. Li, and J. Liu (2019), Composition, mineralogy and chronology of mare basalts and non-mare materials in Von Kármán crater: landing site of the Chang'E− 4 mission, *Planetary and Space science*, *179*, 104741.Liu, Z., K. Di, J. Li, J. Xie, X. Cui, L. Xi, W. Wan, M. Peng,

B. Liu, and Y. Wang (2020), Landing site topographic mapping and rover localization for Chang'e-4 mission, *Science China Information Sciences*, *63*(4), 1-12.Massironi, M., G. Cremonese, S. Marchi, E. Martellato, S. Mottola, and R. J. Wagner (2009), Mercury's geochronology revised by applying Model Production Function to Mariner 10 data: Geological implications, *Geophysical Research Letters*, *36*(21).Melosh, H. J. (1989), Impact cratering: A geologic process, *New York: Oxford University PressOxford: Clarendon Press*, 1-255.Minton, D. A., C. I. Fassett, M. Hirabayashi, B. A. Howl, and J. E. Richardson (2019), The equilibrium size-frequency distribution of small craters reveals the effects of distal ejecta on lunar landscape morphology, *Icarus*, *326*, 63-87.Molaro, J., and S. Byrne (2012), Rates of temperature change of airless landscapes and implications for thermal stress weathering, *Journal of Geophysical Research (Planets)*, *117*(E10), E10011.Povilaitis, R., M. Robinson, C. Van der Bogert, H. Hiesinger, H. Meyer, and L. Ostrach (2018), Crater density differences: Exploring regional resurfacing, secondary crater populations, and crater saturation equilibrium on the moon, *Planetary and Space Science*, *162*, 41-51.Qiao, L., Z. Ling, X. Fu, and B. Li (2019), Geological characterization of the Chang'e-4 landing area on the lunar farside, *Icarus*, *333*, 37-51.Richardson, J. E. (2009), Cratering saturation and equilibrium: A new model looks at an old problem, *Icarus*, *204*(2), 697-715.Salaün, Y., R. Marlet, and P. Monasse (2017), Line-based robust SfM with little image overlap, paper presented at 2017 International Conference on 3D Vision (3DV), IEEE.Thomson, B. J., E. B. Grosfils, D. B. J. Bussey, and P. D. Spudis (2009), A new technique for estimating the thickness of mare basalts in Imbrium Basin, *Geophysical Research Letters*, *36*(12).Wilhelms, D. E., F. John, and N. J. Trask (1987), The geologic history of the Moon*Rep. 2330-7102*.Wood, C., J. Head, and M. Cintala (1977), Crater degradation on Mercury and the moon-Clues to surface evolution, paper presented at Lunar and Planetary Science Conference Proceedings.Wu, B., F. Li, H. Hu, Y. Zhao, Y. Wang, P. Xiao, Y. Li, W. C. Liu, L. Chen, and X. Ge (2020), Topographic and Geomorphological Mapping and Analysis of the Chang'E-4 Landing Site on the Far Side of the Moon, *Photogrammetric Engineering & Remote Sensing*, *86*(4), 247-258.Xiao, Z., and R. G. Strom (2012), Problems determining relative and absolute ages using the small crater population, *Icarus*, *220*(1), 254-267.Xiao, Z., and S. C. Werner (2015), Size-frequency distribution of crater populations in equilibrium on the Moon, *Journal of Geophysical Research: Planets*, *120*(12), 2277-2292.Xie, M., T. Liu, and A. Xu (2020), Ballistic Sedimentation of Impact Crater Ejecta: Implications for the Provenance of Lunar Samples and the Resurfacing Effect of Ejecta on the Lunar Surface, *Journal of Geophysical Research (Planets)*, *125*(5), e06113.Xie, M., Z. Xiao, and A. Xu (2019), Time-dependent production functions of lunar simple craters on layered targets with consideration of topographic degradation, *Geophysical Research Letters*, *46*(20), 10987-10996.Xie, M., M. H. Zhu, Z. Xiao, Y. Wu, and A. Xu (2017), Effect of topography degradation on crater size-frequency distributions: Implications for populations of small craters and age dating, *Geophysical Research Letters*, *44*(20), 10,171-110,179.Yang, C., H. Zhao, L. Bruzzone, J. A. Benediktsson, Y. Liang, B. Liu, X. Zeng, R. Guan, C. Li, and Z. Ouyang (2020), Lunar impact crater identification and age estima-

tion with Chang'E data by deep and transfer learning, *Nature Communications*, *11*(1), 1-15.